

PSFC/JA-01-34

**Double Transport Barrier Experiments on
Alcator C-Mod**

S.J. Wukitch, R.L. Boivin, P.T. Bonoli, C.L. Fiore, R.S. Granetz,
M.J. Greenwald, A.E. Hubbard, I.H. Hutchinson, Y. In,¹ J. Irby,
Y. Lin, E.S. Marmor, D. Mossessian, M. Porkolab, G. Schilling,²
J.E. Rice, J.A. Snipes, S.M. Wolfe and the Alcator C-Mod Group

December 2001

Plasma Science and Fusion Center
Massachusetts Institute of Technology
Cambridge, MA 02139 USA

¹University of Idaho, Moscow, Idaho

²Princeton Plasma Physics Laboratory, Princeton, NJ

This work was supported by the U.S. Department of Energy, Cooperative Grant No. DE-FC02-99ER54512. Reproduction, translation, publication, use and disposal, in whole or in part, by or for the United States government is permitted.

Submitted for publication to *Physics of Plasmas*.

Double transport barrier experiments on Alcator C-Mod

S. J. Wukitch, R. L. Boivin, P.T. Bonoli, C.L. Fiore, R.S. Granetz, M. J. Greenwald, A. E. Hubbard, I. H. Hutchinson, Y. In,⁺ J. Irby, Y. Lin, E. S. Marmor, D. Mossessian, M. Porkolab, G. Schilling,* J. E. Rice, J.A. Snipes, S. M. Wolfe, and the Alcator C-Mod group.

Plasma Science and Fusion Center, Massachusetts Institute of Technology, Cambridge, Massachusetts 02139

+University of Idaho, Moscow, Idaho

*Princeton Plasma Physics Laboratory, Princeton, New Jersey

Abstract

Double transport barrier modes (simultaneous core and edge transport barrier) have been observed with off-axis ion cyclotron range of frequencies (ICRF) heating in the Alcator C-Mod tokamak [I. H. Hutchinson et al., Phys. Plasmas **1**, 1511(1994)]. An internal transport barrier (ITB) is routinely produced in enhanced D_α H-mode (EDA) discharges where the minority ion cyclotron resonance layer is at $r/a \sim |0.5|$ during the current flat top phase of the discharge. The density profile becomes peaked without the presence of a particle source in the plasma core and continues to peak until the increased core impurity radiation arrests the improved energy confinement, ultimately leading to a barrier collapse. With the addition of moderate (0.6 MW) central ICRF heating, the double barrier mode was maintained for as long as the ICRF power was applied and modeling shows that the internal thermal barrier was maintained throughout the discharge. The presence of sawteeth throughout most of the ITB discharge allows sawtooth-induced heat pulse analysis to be performed. This analysis indicates that there is an abrupt radial discontinuity in the heat pulse time to peak profile when an ITB is present. Furthermore, this discontinuity appears to move into the core plasma from the edge region in about 0.2 sec, several confinement times. The deduced thermal diffusivity, χ^{hp} , indicates a barrier exists in the electron thermal transport, the barrier is limited to a narrow radial region, and the transport is unaffected outside this narrow radial extent.

I. Introduction

Discharges with internal transport barriers (ITB) exhibit improved confinement in one or more of the thermal, particle, or momentum channels for either the ions or the electrons in the plasma core. These discharges exhibit significantly reduced transport often approaching neoclassical levels.^{1,2} Studies of internal transport barriers in thermally equilibrated plasmas at high density are of practical importance to a future fusion reactor, and are also of fundamental physics interest. Like conditions expected in a reactor, these plasmas have no central fueling, no external torques, and equilibrated temperatures. The lack of a central fueling and external momentum source is of interest because among the variety of techniques developed to access an ITB, most utilize neutral beam injection that provides both. At high densities that are typical of expected reactor conditions, beam penetration is expected to be a significant challenge. Therefore, techniques for triggering an ITB with central momentum and particle sources may not be applicable. Finally for a reactor grade plasma, the electron and ion temperatures are expected to be equilibrated. In this regime, the ion temperature gradient mode is more unstable than the case where ion temperature (T_i) is greater than the electron temperature (T_e) as suggested by theoretical considerations and transport trends observed on DIII-D and ASDEX-U.^{3,4}

In Alcator C-Mod, ITBs in plasmas with conditions similar to those expected in reactor plasmas have been investigated. Here we report the observation and transport analysis of high density, double transport barrier discharges with an ITB created with off-axis ICRF heating, and controlled with additional central ICRF power. These discharges are characterized by an edge transport barrier (ETB), associated with the enhanced D_α (EDA) H-mode, and peaked density profile associated an ITB.^{5,6,7} In an EDA H-mode, the particle transport is sufficiently enhanced over the ELM-free (edge localized mode) H-mode level to result in stationary density and impurity levels.⁸ Previously, C-Mod ITB experiments have focused upon heating during current ramp-up with ICRF,⁹ pellet enhanced performance mode,¹⁰ and the enhanced neutron mode.¹¹ The latter is an ITB mode initiated by a transition from H to L-mode in which the density profile becomes peaked resulting from the ETB collapse. In earlier double barrier experiments, the ITB formation was unreliable and appeared to be triggered by a local density gradient resulting from ELM activity.¹²

In the following, section II provides a description of the experimental setup; section III presents the experimental observations of ITB formation and control. The results of TRANSP modeling of a representative discharge are discussed in section IV. The sawtooth-induced heat pulse analysis on a few representative ITB discharges will be presented and discussed in section V. We conclude with a summary of the results in section VI.

II. Experimental Description and Diagnostics

Alcator C-Mod is a compact (major radius $R=0.67$ m, minor radius $a=0.22$ m), high field ($B_t < 8.1$ T) divertor tokamak.¹³ The discharges analyzed here are single null EDA H-mode D(H) minority (minority in parentheses) ion cyclotron range of frequency (ICRF) heated with the H/D ratio typically 5-10%. The on-axis toroidal fields, B_T , used were 4.5 T and 5.4 T. The plasma current, I_p , was 0.7-0.8 MA and the target (density prior to H-mode transition) average density, \bar{n}_e , was $\sim 1.5 \times 10^{20} \text{ m}^{-3}$. The (ICRF) heating power is coupled to the plasma via three fast wave antennas (2 two-strap and a four-strap) operated in heating phasing. The two-strap antennas are operated at 80 MHz and together couple up to 3 MW in these discharges. The four-strap antenna is operated at 70 MHz and up to 2 MW was injected. For the 4.5 T discharges, the minority cyclotron resonance is located on the high field side of the magnetic axis at $r/a \sim -0.5$ for 80 MHz and the low field side at $r/a \sim +0.15$ for 70 MHz. For 5.4 T discharges, the 70 and 80 MHz minority cyclotron resonance's are located on the low field at $r/a \sim +0.5$ and the high field side at $r/a \sim -0.15$, respectively. If the minority cyclotron resonance is located at inside $r/a < |0.2|$, this heating will be referred to as central, and for $r/a > |0.2|$ the heating will be referred to as off-axis.

Results from a set of core diagnostics to measure electron temperature and density, impurity ion temperature and density, impurity ion rotation, visible bremsstrahlung emissivity, radiated power, soft x-ray emissivity, and global neutron rate will be presented. The electron temperature profiles are obtained from two grating polychromator electron cyclotron emission (ECE) diagnostics.¹⁴ A core and edge Thomson scattering system records the electron temperature and density profiles. Density profiles are also obtained from multichord interferometry using the edge Thomson scattering to account properly for the plasma edge region and from a high spatial and temporal resolution visible bremsstrahlung, VB, emission diagnostic.¹⁵ To unfold the density profile from the VB-emission, the effective charge, Z_{eff} , is estimated by comparing the central VB-emissivity to central Thomson scattering density. Assuming a flat Z_{eff} profile and also accounting for a weak electron temperature dependence, the square root of the emissivity is the electron density profile. The ion temperature profile is

obtained for $r/a < 0.5$ from a scannable array of 5 high spectral resolution x-ray spectrometers (HIREX).¹⁶ The central toroidal impurity rotation is obtained from x-ray spectra recorded by a spatially fixed tangentially viewing von Hamos type crystal x-ray spectrometer and assumed to represent the plasma rotation.¹⁷ The soft x-ray signals are measured using a diode array with 50% transmission at 2 keV.¹⁸ The spatial resolution, mapping the tangential flux surface position to the mid-plane, is 1-2 cm. A high-resolution diode based bolometer array is used to measure the total radiated power profile.¹⁹ The total neutron flux is measured using a bank of He³ filled proportional counters surrounded by polyethylene moderator, cross-calibrated to an absolutely calibrated neutron diagnostic.²⁰

III. Double Transport Barrier Experiments

In recent experiments, the conditions required to create an ITB in EDA H-mode plasmas have been investigated.²¹ A typical discharge ($B_T = 4.5$ T, $I_p = 0.8$ MA) with 2 MW off-axis ICRF heating is shown in Fig. 1. The 80 MHz ICRF minority resonance is at $r/a \sim 0.5$ with 70 MHz central ICRF added late in the discharge (1.25 sec) at the 0.6 MW level. With the application of off-axis ICRF at 0.7 sec, the plasma immediately transitions from L-mode to EDA H-mode. In a typical EDA H-mode, the average density reaches a steady value. In discharges with an ITB, the average density continues to increase which is evident from $t > 0.8$ sec till the application of central ICRF in the discharge shown. In ITB discharges, the neutron rate also continues to increase. During the ITB+EDA phase ($t = 1.2$ sec), the neutron rate becomes ~ 2.5 times larger compared to the initial EDA phase ($t = 0.8$ sec). The central ion temperature remains constant throughout the off-axis heating phase while the density is increasing. Finally, the central toroidal rotation, typically in the co-current direction in EDA discharges, decreases and often reverses direction. While the trigger for the development of the ITB is unknown, the ITB has not been observed in L-mode, nor ELM-free H-mode, nor centrally heated EDA H-mode discharges suggesting an EDA H-mode with the minority resonance $r/a \sim |0.5|$ is a necessary condition. Furthermore, the power threshold for ITB formation appears to be no more than the power required to establish the EDA H-mode. The ITB development and sustainment appears to be influenced by the level of central heating. With the application of moderate (< 0.6 MW) central heating, the peaked density profile can be sustained for as long as the ICRF is applied as shown in the Fig.1 for $t > 1.25$ sec. Furthermore, the central rotation begins to increase with the application of central heating. Examination of the density and radiation profiles, shown in Fig. 2, indicates the density and impurity accumulation are arrested by the central heating. By varying the delay of the application of moderate (0.6 MW) central heating, the density can be arrested at any value. For central heating power > 0.6 MW, the density profile becomes less peaked.¹⁸

Control of the ITB development by central heating is speculated to be the result of destabilizing some additional microturbulence modes. From the literature, ITG modes are well known to be stabilized by a peaked density profile, whereas trapped electron modes (TEM) are known to be destabilized by density gradients.²² It is speculated that TEMs are destabilized as the central temperature is increased by the addition of the central power. Further experiments and analysis are required to determine the mechanism responsible for arresting the density accumulation with additional central heating.²³

The role of the ICRF in formation and control of the ITB is ambiguous. In ohmic EDA H-modes, ITBs are also observed, suggesting the ICRF does not play a direct role in the formation of the ITB. The barrier foot appears to nearly coincide with the minority resonance in the experiments to date at $r/a \sim |0.5|$. Further experiments to attempt to separate minority

resonance position and barrier foot need to be pursued to properly answer whether the minority resonance position is influencing the location of ITB foot.

IV. TRANSP Modeling and Discussion

Using TRANSP, the power balance particle flux, Γ , and heat flux, q , are found by solving the magnetic field diffusion equation and the particle and energy balance equations, given experimental n_e , T_e and T_i profiles and magnetic equilibria.²⁴ The model assumes the plasma is toroidally symmetric and the density, temperature, and current density are flux surface quantities. This model reduces the transport problem to the radial dimension.

For clarity, the particle and power balance equations are shown below:

$$\begin{aligned}\nabla \cdot \Gamma_j &= S_j - \frac{\partial n_j}{\partial t} \\ \nabla \cdot q_j &= Q_j + \frac{3}{2} n_j \frac{\partial T_j}{\partial t}\end{aligned}\tag{1}$$

where j refers to species, S is the particle source, and Q is the thermal source. In C-Mod discharges, the core particle source is zero; thus, pinch terms must be playing an important role in the development of peaked density profiles. Using calculated Γ and q , D is calculated using the $\Gamma = -D\nabla n + v_e n$, where v_e is the pinch velocity and $q = -\chi \nabla T$. Although the electron, χ_e , and ion, χ_i , thermal diffusivities are available, we will use $\chi_{\text{eff}} = (n_e \chi_e \nabla T_e + n_i \chi_i \nabla T_i) / (n_e \nabla T_e + n_i \nabla T_i)$. This form is used because of the strong coupling between electrons and ions in C-Mod plasmas and it eliminates the need to calculate accurately the ICRF power partition between electrons and ions.

The most obvious experimental evidence for the presence of a thermal barrier in these ITB discharges is the fact that the central T_i remains constant as the central density increases. To investigate further the thermal and particle transport properties of these ITB discharges, the TRANSP analysis of a representative discharge shown in Fig 1 is presented.

For the TRANSP analysis, the experimental T_i , T_e , and n_e profiles are required; however, the experimental T_i profile is incomplete. Two models for the T_i profile were constructed and were analyzed yielding similar transport results. One model used the measured partial T_i profile, $r/a < 0.5$, measured in four consecutive, similar discharges. The T_i profile is assumed to be equal to the T_e profile for $r/a > 0.5$. The T_i profile is interpolated in time by scaling the profile by the ratio of the central T_i deduced from the neutrons and impurity T_i . The other method assumes $T_i = T_e$ and the T_e profile is determined from ECE data. With the sawtooth mixing included, the total neutron rate calculated from TRANSP is in good agreement with experimental value suggesting the constructed T_i and T_e profiles used in the modeling are consistent with the experimental data. The ICRF power deposition profile is calculated using a bunched averaged Fokker Planck code coupled to the full wave code TORIC.²⁵ The resulting power deposition profile for both the off-axis heating and the combined central and off-axis heating are shown in Fig 3. The effective thermal diffusivity, χ_{eff} , profile for the L-mode, ITB with off-axis ICRF heating, and ITB with off-axis and central ICRF are shown in Fig 4. Compared with the L-mode case, the energy confinement is improved significantly for the core region inside $r/a < 0.5$, in agreement with the location of the particle barrier. Note the confinement is improved over the entire region shown as a result of the transition from L-mode to the ITB + EDA H-mode. The analysis suggests that the thermal barrier is maintained even after the central ICRF is added.

Without a central particle source, the central density rate of rise suggests the outward diffusion is exceeded by an inward pinch. The neoclassical Ware pinch velocity,²⁶ v_w , is calculated by TRANSP to be of order the inferred density pinch velocity, v_e , suggesting it could account for the density accumulation. A comparison of the particle and Ware pinch velocities is shown in Fig. 5a. In Fig. 5b, the calculated particle diffusivity decreases across the whole plasma cross-section during the ITB compared to L-mode. With additional central power, the density accumulation is arrested suggesting the outward diffusion balances the inward Ware pinch. As the central heating is increased to 2 MW, the peaked density profile is steadily reduced indicating that particle transport is increasing with central heating.

V. Sawtooth-induced Heat Pulse Analysis and Discussion

Since the sawtooth instability is present throughout these ITB discharges, the sawtooth-induced heat pulse propagation can be used to study the thermal transport.^{27,28,29,30} Transient transport experiments using ITB formation to deduce the χ^{hp} have been reported.³¹ This paper is the first report of using sawtooth-induced heat pulse to investigate ITB thermal transport characteristics. This technique will allow us to probe directly χ_e and probe ITB dynamics. In the discussion below, χ_{eff} will be used to represent the thermal diffusivity calculated from the TRANSP and χ^{hp} is the thermal diffusivity calculated from the sawtooth-induced heat pulse.

In this paper, the sawtooth-induced heat pulse is measured via soft x-rays or electron cyclotron emission and the time-to-peak is recorded as a function of radius. Outside the near field region (defined to be $1.4 \times \text{mixing radius}$, r_m , where the pulse propagation could reflect convection dominated transport) and away from the edge region (defined to be $r^2 < 0.7a^2$, a is minor radius, where pulse pile up could influence the deduced χ^{hp}) χ^{hp} is given by:²³

$$\chi^{hp} = \frac{\Delta r^2}{9\Delta t_p} \quad (2)$$

where r is minor radius and t_p is the time-to-peak. The t_p for a given sawtooth heat pulse in an x-ray channel is found by fitting a function to the data and finding the delay from the sawtooth crash to the time at which the fitted function is a maximum. The error is estimated by the width at 0.9 of the maximum, a measure of pulse sharpness. One also can solve the diffusion equation in cylindrical coordinates using a finite difference method given as:²³

$$\frac{3}{2} n_e \frac{\partial \tilde{T}_e}{\partial t} = \frac{1}{r} \frac{\partial}{\partial r} \left[r n_e \chi_e^{hp} \frac{\partial \tilde{T}_e}{\partial r} \right] \quad (3)$$

where n_e is the electron density.

Shown in Fig 6 is a zoomed view of the soft x-ray brightness data for a select number of channels from two EDA discharges where an ITB formed in one and not the other. These discharges are similar in plasma current and density, but with $B_T = 4.9$ T and $B_T = 4.5$ T in the EDA H-mode and ITB discharges, respectively. The difference in B_T field results in the minority resonance position, located at $r/a \sim 0.3$ during the EDA discharge, moving to $r/a \sim 0.5$ for the ITB discharge. In the EDA case, there is a steady increase in the t_p with radial position. In the ITB case, one can readily observe the heat pulse delay between channels at $r=9.8$ cm and $r=11.0$ cm. This delay is reflected in the radial t_p profiles shown in Fig 7 for each discharge. One can observe a significant radial discontinuity in the t_p profile for the ITB discharge and the location of the discontinuity coincides with the observed foot of the ITB. To verify that the soft

x-ray time-to-peak signal reflects the heat pulse, a comparison of the t_p profiles from soft x-ray and ECE for another ITB discharge, where the ECE was not cut off, is shown in Fig 8. There is good agreement as to the location of the discontinuity and even the values of the t_p at different radial positions, supporting the use of t_p data from the soft x-rays to deduce χ^{hp} .

To characterize the thermal transport, we numerically solve Eq. 3 assuming a flat χ^{hp} profile with a narrow radial region of reduced χ^{hp} and a flat density profile. The boundary conditions are $\tilde{T}_e(0, t) = \tilde{T}_e(\sqrt{2} * r_{mix}, t)$ and $\tilde{T}_e(a, t) = 0$. In Fig 9, the experimental and simulated t_p profiles for a shot with weak density peaking are shown. The t_p profile from the simulated data is in good agreement, using $\chi^{hp}=4 \text{ m}^2/\text{sec}$ outside the barrier and $\chi^{hp}=0.4 \text{ m}^2/\text{sec}$, with experimental values. Thus, the discontinuity in t_p profile can be interpreted to be a result of a localized transport barrier. This discharge was selected because the near field effect is minimized, with only the point at 0.07 m in the near field region. It should be noted that this value of χ^{hp} is about a factor of 4 times the typical EDA H-mode χ_{eff} value. The transport barrier region is less than 0.01 m, the limit of the diagnostic resolution. This result suggests a higher resolution x-ray or ECE diagnostic will be required to probe the local barrier structure.

Returning to the 4.5 T, ITB discharge, three t_p profiles are shown in Fig 10 and one can readily observe the transport barrier is initiated in the edge region and propagates into the plasma core. In addition, the transport outside this narrow radial region appears to be unchanged except for the last time point ($t=1.03 \text{ sec}$). In this case, the transport in the region between the barrier and the edge appears to have degraded. However, the heat pulse signal beyond the transport barrier is particularly weak at this time and may not accurately reflect the diffusive heat pulse transport. The transport barrier propagation can perhaps be compared to the VH-mode (Very High confinement mode) observed on DIII-D,³² JET,³³ and TUMAN-3.³⁴ For example in DIII-D, the VH-mode is characterized by the development of a broad transport barrier initiated in the edge region where the barrier front then continues to propagate radially inward, occupying the plasma region for $\rho > 0.6$. The common feature is the barrier initiation in the edge region (the ITB presented here appears to be a narrow transport barrier whereas the VH mode was characterized by a wide transport barrier). According to initial modeling of the VH-mode barrier front propagation, the transport barrier is initiated at the plasma edge and a radially propagating transition front develops as a result of spatially propagating transition instability.³⁵ We speculate that such a model could be consistent with the results reported here. Interestingly, the model suggests the barrier initiated at the plasma edge should propagate to the periphery of the power deposition region. This is roughly consistent with the location of the foot of the barrier and suggests a path to control the location of the foot of the ITB, the subject of future research.

Referring to Fig 10 again, the barrier transit time decreases as the barrier moves into the plasma core. The first t_p profile, in diamonds, is measured $\sim 0.1 \text{ sec}$ after the transition from L to H-mode. Approximately $\sim 0.1 \text{ sec}$ later (triangles), the transport barrier has moved inward $\sim 0.03 \text{ m}$ corresponding to a propagation velocity of $\sim 0.4 \text{ m/sec}$. The final t_p profile, indicated by the squares, shows the barrier has propagated a shorter distance, $\sim 0.015 \text{ m}$, with a propagation velocity of 0.12 m/sec . Using the model discussed in the previous paragraph, the relatively slow and discrete barrier propagation suggests it could be modeled using a fluctuation-flow model with spatially varying coefficients (see reference 34). This model suggests two distinct paths for transport barrier evolution. For moderate power levels $P \geq P_{th}$ (P_{th} = H-mode power threshold), a distinct propagating front can be observed while $P \gg P_{th}$ for the transition is predicted to be a nonlocal fluctuation quench or reduction resulting in improved confinement. This suggests

further experiments using higher input power may result in the observation of the latter type of ITB formation.

VI. Conclusions

Double transport barrier modes with simultaneous core and edge transport barrier have been observed with off-axis ICRF heating. An ITB is routinely produced in EDA H-mode discharges where the minority ion cyclotron resonance layer is $r/a \sim |0.5|$. The density profile becomes peaked without the presence of a core particle source. With the addition of central ICRF heating, the double barrier mode was maintained for as long as the ICRF was applied and TRANSP analysis shows that the internal energy barrier was maintained throughout the discharge. The presence of sawteeth allows transient transport analysis to be performed in these discharges. This analysis indicates that there is an abrupt radial discontinuity in the heat pulse time to peak profile when an ITB is present. Furthermore, this discontinuity appears to move into the core plasma from the edge region. Modeling indicates the barrier region is limited to a narrow radial region and outside this barrier the transport is unaffected.

VII. Acknowledgements

This work is supported by Department of Energy Coop. Agreement DE-FC02-99ER54512. The authors would like to thank the Alcator C-Mod engineering and technical staff for providing regular and reliable experimental operation.

Figure Captions

Figure 1. Representative ITB discharge with 2 MW of off-axis ICRF heating throughout the discharge and 0.6 MW of central ICRF heating applied at 1.25 sec used for TRANSP modeling. Summary traces are ICRF power, stored plasma energy, average density, neutron rate, ion temperature and toroidal rotation.

Figure 2. (a) Density profile evolution at 0.1 sec intervals for representative ITB discharge showing central density accumulation until it is arrested with the application of the central ICRF. (b) Impurity profile evolution for representative ITB discharge showing increased radiated power until it is arrested with the application of the central ICRF.

Figure 3. Calculated ICRF power deposition profile for both the off-axis only and central+off-axis heating scenarios with $B_T=4.5$ T.

Figure 4. Comparison of effective thermal diffusivity shows improved diffusivity inside $r/a < 0.5$ during ITB phase in good agreement to the position of particle barrier foot.

Figure 5. (a) Calculated Ware pinch velocity, v_w , is consistent with the particle pinch velocity, v_e , calculated by TRANSP. (b) The particle diffusivity, D , decreases across the plasma cross section compared to the L-mode phase and is a minimum near the location of the particle barrier foot.

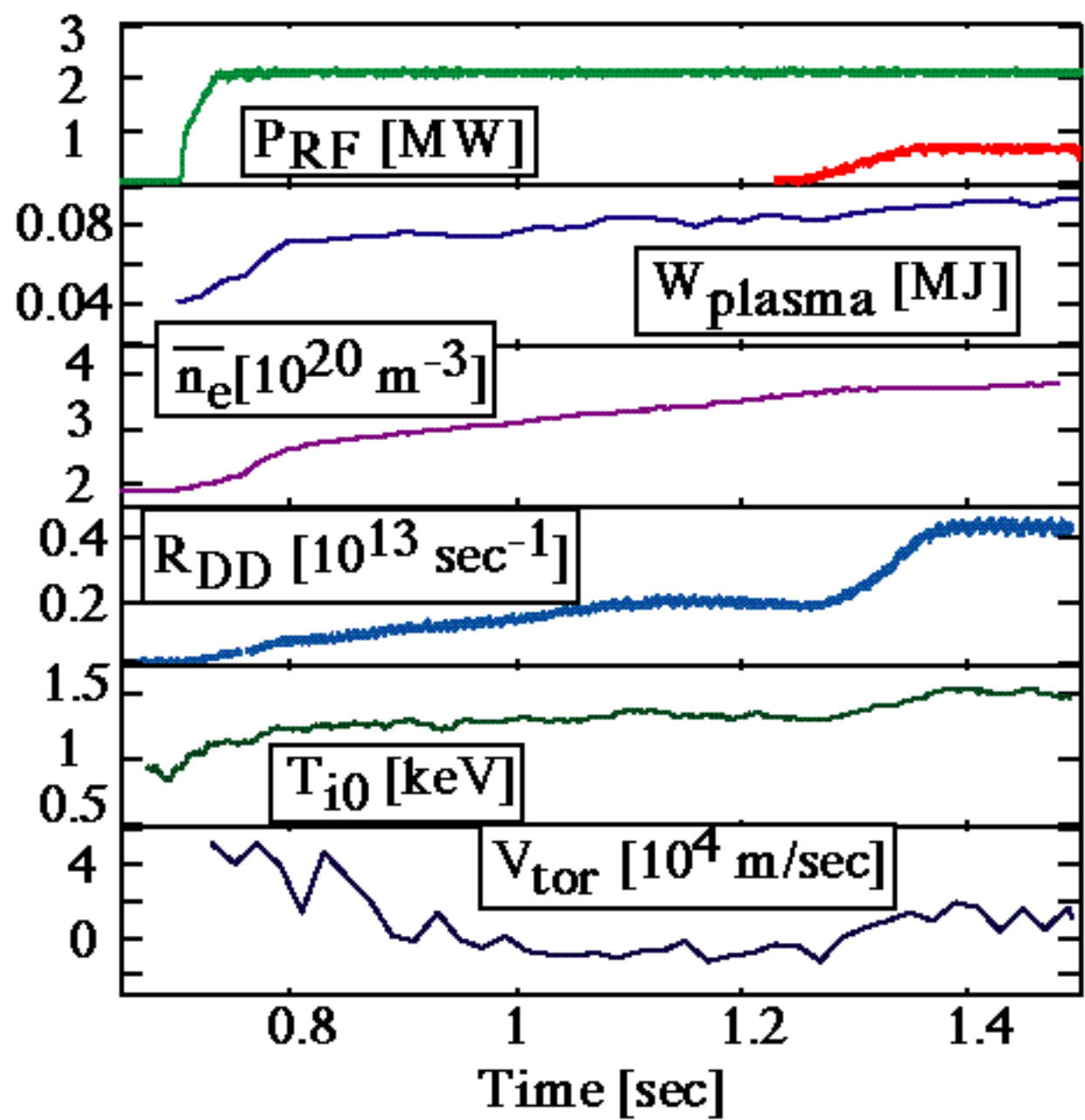
Figure 6. Soft x-ray brightness cords comparing the sawtooth-induced heat pulse propagation of two EDA H-mode discharges in which an ITB forms in one of discharges shown in gray. Note the pulse delay between $r=9.8$ cm and $r=11.0$ cm.

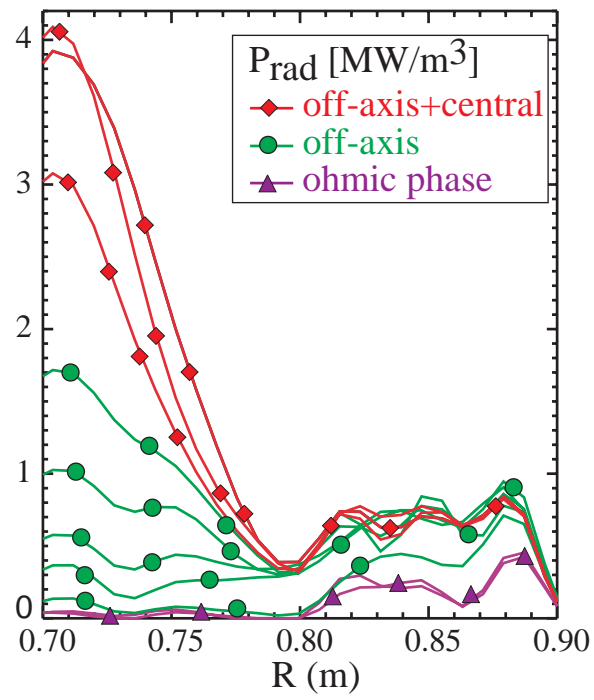
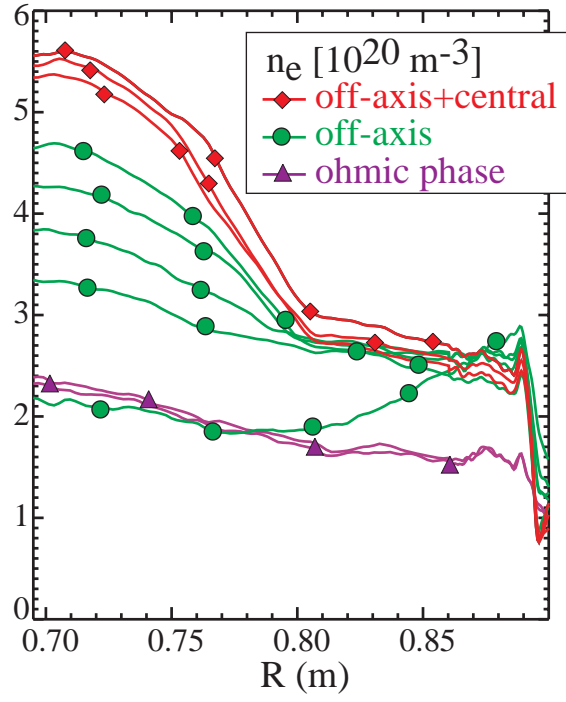
Figure 7. Time-to-peak radial profile comparing the ITB (squares) to EDA discharge (diamonds) where the bar indicates the radial location of the foot of the particle barrier.

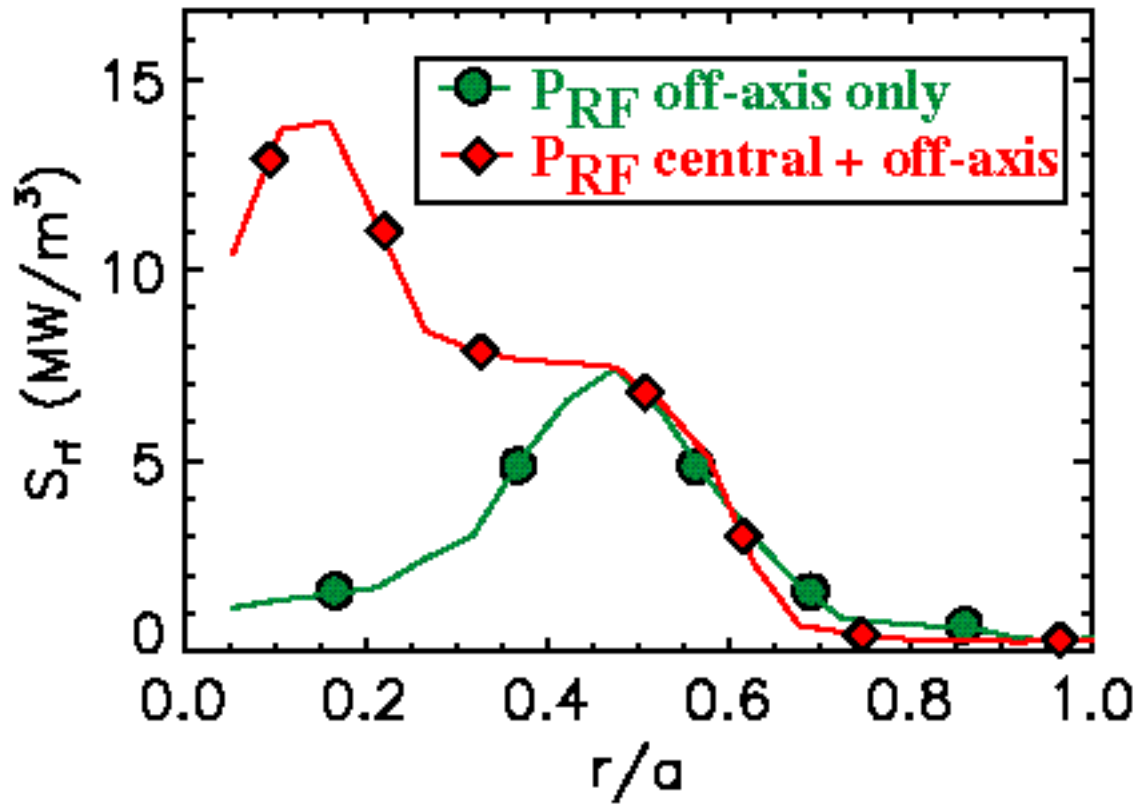
Figure 8. Comparison time to peak data from sawtooth-induced heat pulse measured by ECE (diamonds) and soft x-rays (squares) for an ITB discharge at 5.4 T showing good agreement.

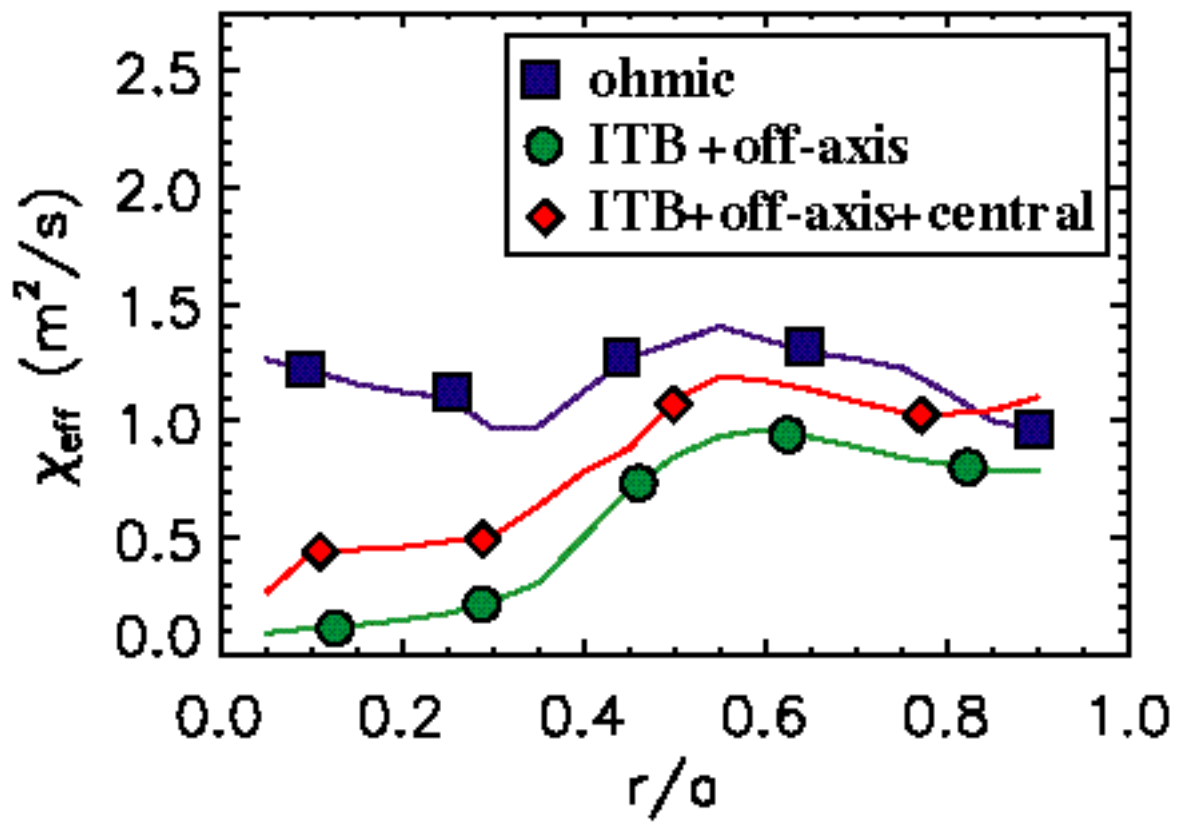
Figure 9. Comparison of the experimental (squares) and simulation (diamonds) time-to-peak data shows good agreement for the assumed χ^{hp} profile (solid line). This indicates that the region of improved confinement is restricted to a narrow radial layer and outside of this region there is little evidence of improved transport.

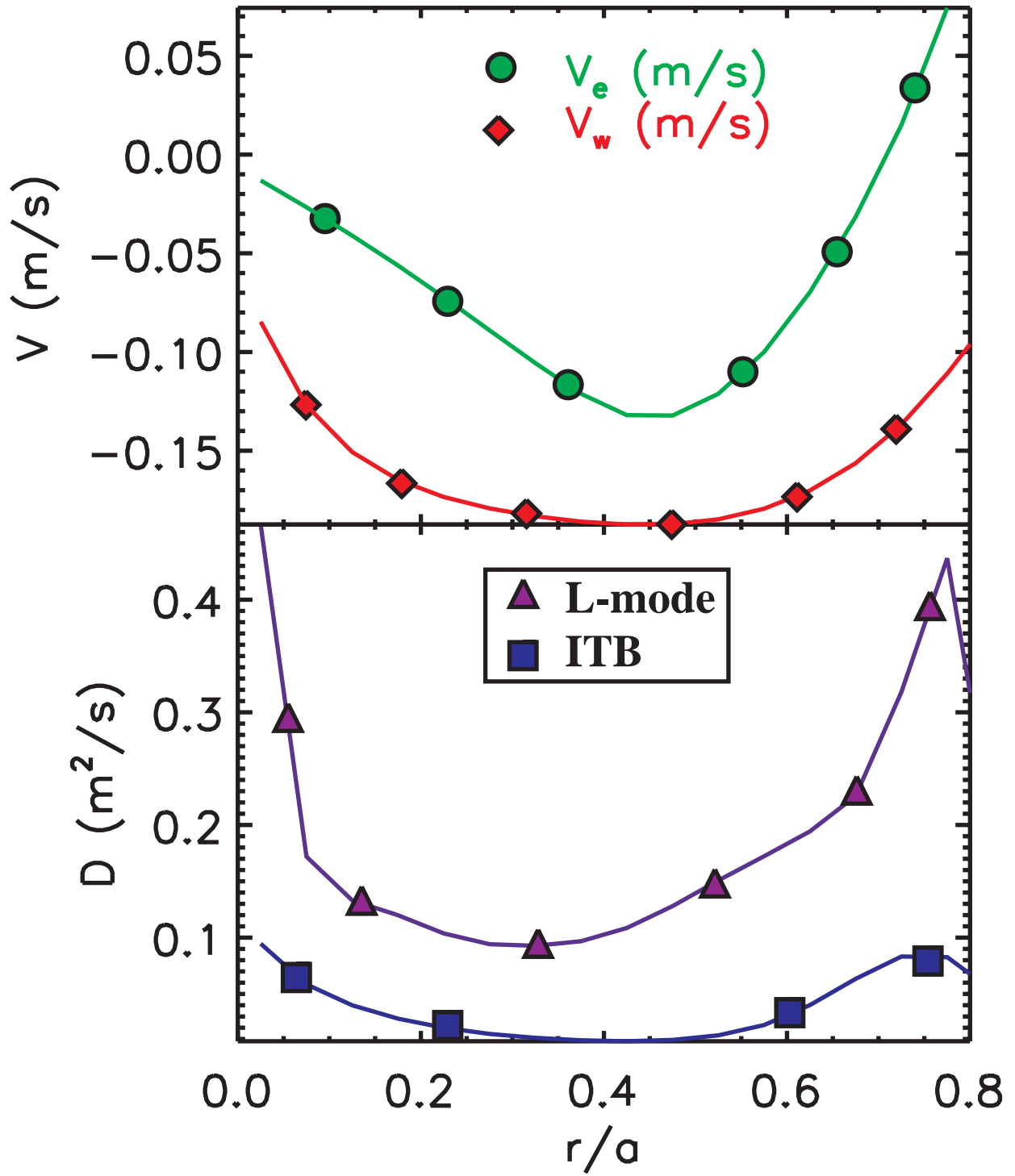
Figure 10. Time evolution of the radial time to peak profile for ITB discharge shows an inward propagation of the discontinuity. The first time point (diamonds) is 0.1 sec after the L->H transition (0.7 sec), the next profile (triangles) is taken at 0.9 sec, and the final profile (squares) shown is taken at 1.03 sec.

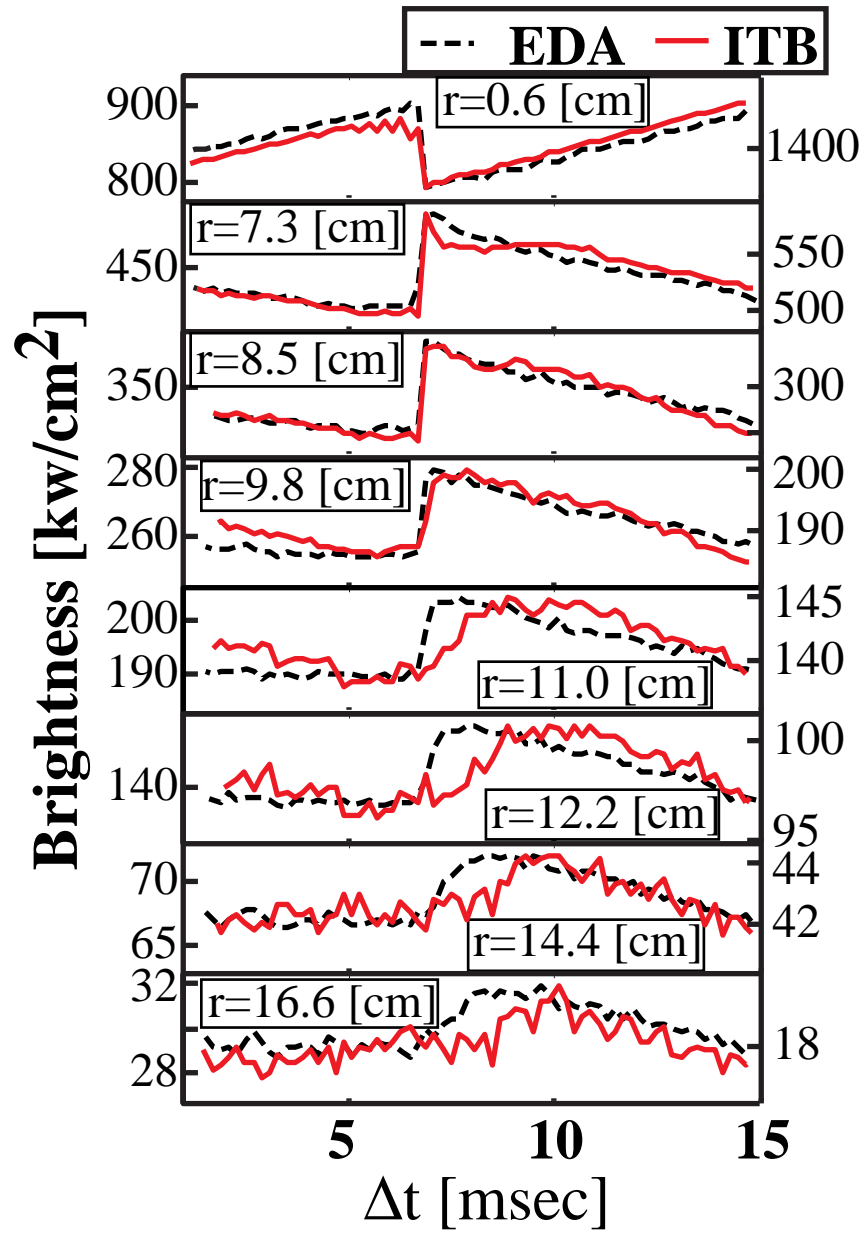


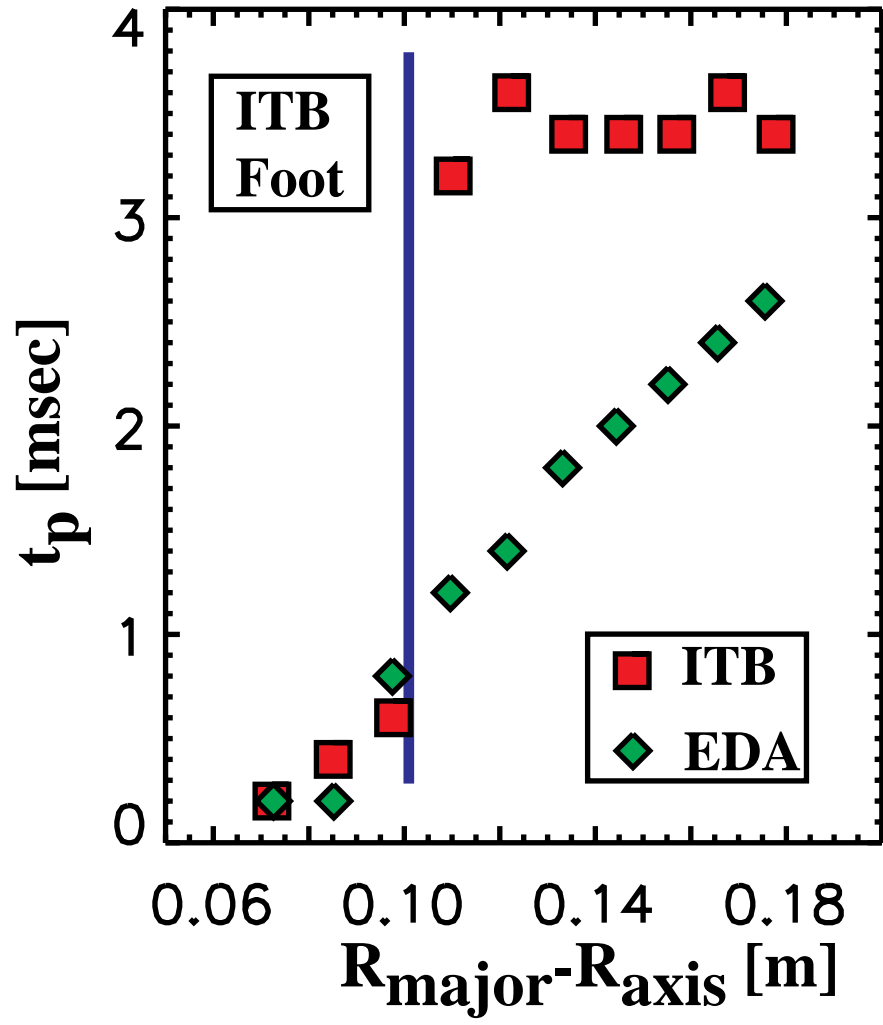




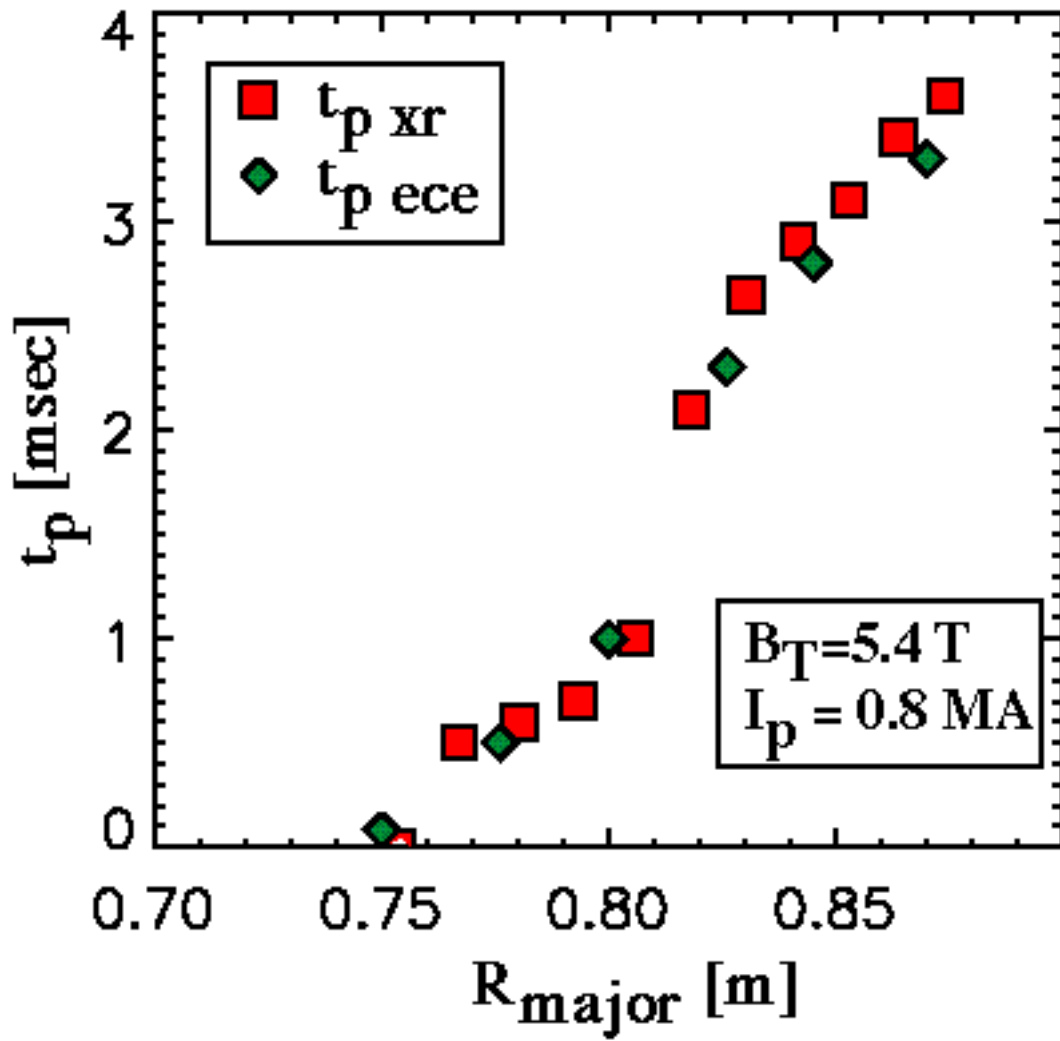


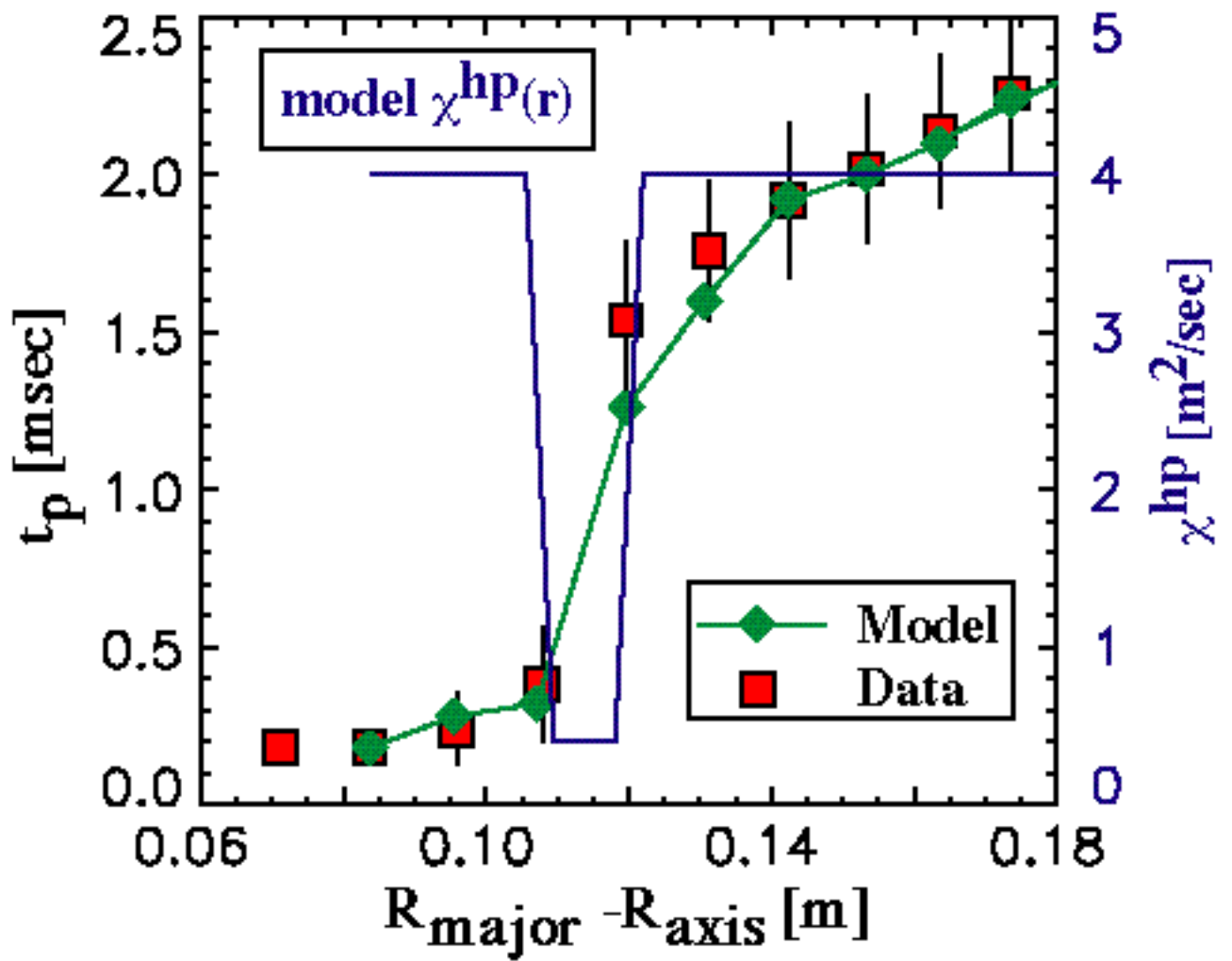


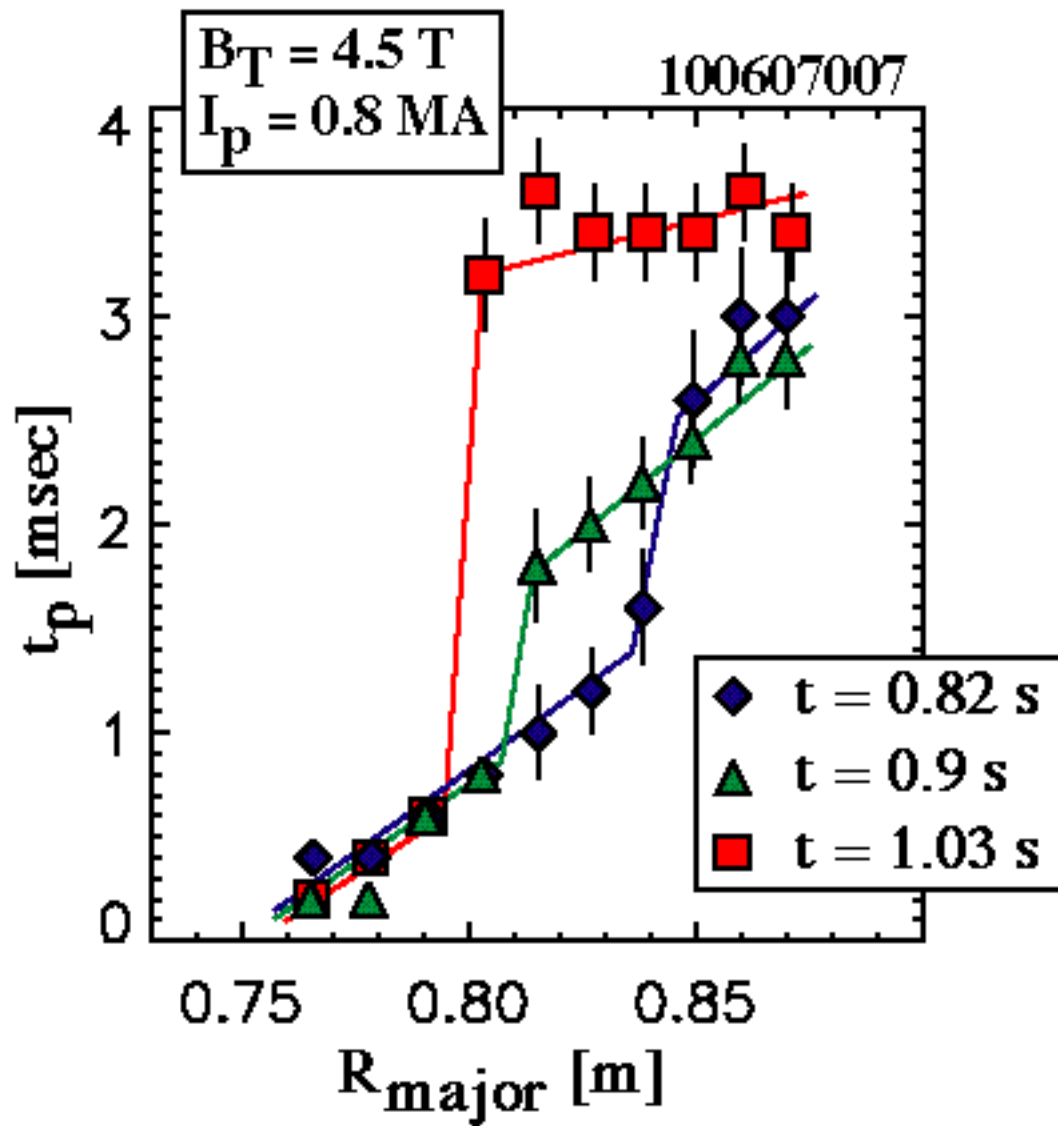




1010801027







References

- ¹ F. Levinton, M.C. Zarnstorff, S.H. Batha, *et al.*, Phys. Rev. Lett. **75**, 4417 (1995).
- ² E.J. Strait, L.L. Loa, M.E. Mauel, *et al.*, Phys. Rev. Lett. **75**, 4421 (1995).
- ³ C.C. Petty, M. R. Wade, J.E. Kinsey, *et al.*, Phys. Rev. Lett. **83**, 3661 (1999).
- ⁴ K. Lackner, S. Guenter, F Jenko, A. Peeters and R. Wolf, Plasma Phys. Control. Fusion **42**, B37 (2000).
- ⁵ F.X. Soldner, Yu.F. Baranov, D.V. Bartlett, *et al.*, Nuclear Fusion **39**, 407 (1999).
- ⁶ O. Gruber, R. Wolf, H.-S. Bosch, *et al.*, Nuclear Fusion **40**, 1145 (2000).
- ⁷ C.M. Greenfield, K. H. Burrell, J. C. DeBoo, *et al.*, Phys. Rev. Lett. **86**, 4544 (2001).
- ⁸ M. Greenwald, R.L. Boivin, P.T. Bonoli, *et al.*, Physics of Plasmas **6**, 1943 (1999).
- ⁹ M. Porkolab, R.L. Boivin, P.T. Bonoli *et al.*, Proceedings of the Contrib. Papers, 24th European Phys. Society Conference on Plasma Physics and Contr. Fusion, Berchtesgarnern 1997,(EPS, 1997) Part 2, p 569.
- ¹⁰ Y. Takase, R.L. Boivin, F. Bombarda, *et al.*, Plasma Phys. Control. Fusion **38**, 2215 (1996).
- ¹¹ C.L. Fiore, J.E. Rice, P.T. Bonoli, R.L. Boivin, *et al.*, Physics of Plasmas **8**, 2023 (2001).
- ¹² S.J. Wukitch, P.T. Bonoli, E. Nelson-Melby, *et al.*, Proceedings of Contrib. Papers, 25th European Phys. Society Conference on Plasma Physics and Contr. Fusion , Praha, 1998, (EPS, 1998) Vol 22C, p 707.
- ¹³ I.H. Hutchinson, R. Boivin, F. Bombarda *et al.*, Phys. Plasmas **1**, 1511 (1994).
- ¹⁴ A. Hubbard , R. L . Boivin, R. S. Granetz *et al*, Phys. Plasmas **5**, 1744 (1997).
- ¹⁵ E.S. Marmor, R. L. Boivin, R. S. Granetz, J. W. Hughes, B. Lipschultz, S. McCool, D. Mossessian, C. S. Pitcher, J. E. Rice, and J. L. Terry, Rev. Sci. Instrum. **72**, 940 (2001).
- ¹⁶ J. E. Rice and E. S. Marmor, Rev. Sci. Instrum. **66**, 752 (1995).
- ¹⁷ J. E. Rice, P. T. Bonoli, J. A. Goetz *et al.*, Nucl. Fusion **39**, 1175 (1999).

-
- ¹⁸ R. S. Granetz and L. Wang, in *International School of Plasma Physics-9, 1991, Proceedings of Diagnostics for contemporary Fusion Experiments, Varenna, Italy* (Editrice Compositori, Bologna, 1991) p. 425.
- ¹⁹ R.L. Boivin, R. L. Boivin, J. A. Goetz, E. S. Marmor, J. E. Rice, and J. L. Terry, *Rev. Sci. Instrum.* **70**, 260 (1999).
- ²⁰ C. L. Fiore and R. L. Boivin, *Rev. Sci. Instrum.* **66**, 945 (1995).
- ²¹ J. E. Rice, P.T. Bonoli, E.S. Marmor, *et al.*, "Double Transport Barrier Plasmas in Alcator C-Mod," submitted to *Nucl. Fusion*.
- ²² G.M. Staebler, *Nucl. Fusion* **39**, 815 (2000).
- ²³ P.T. Bonoli, R.L. Boivin, C. Fiore, *et al.*, "Double Transport Barrier Mode in the Alcator C-Mod," submitted to *Phys Rev. Letters*.
- ²⁴ R. Hawryluk, in *Physics of Plasma Close to Thermonuclear Conditions*, (Varenna, 1979), Commission of the European Communities, Brussels, Vol. I, p. 61 (1979).
- ²⁵ M. Brambilla, *Plasma Phys. Control. Fusion* **41**, 1 (1999).
- ²⁶ A.A. Ware, *Phys. Rev. Lett.* **25**, 916 (1970).
- ²⁷ J.D. Callen and G.L. Jahns, *Phys. Rev. Lett.* **38**, 971 (1977).
- ²⁸ M. Soler and J.D. Callen, *Nucl. Fusion* **19**, 703 (1979).
- ²⁹ E.D. Fredrickson, J.D. Callen, K.M. McGuire, *et al.*, *Nucl. Fusion* **26**, 849 (1986).
- ³⁰ N.J. Lopes Cardozo, *Plasma Phys. Control. Fusion* **37**, 799 (1995).
- ³¹ S.V. Neudatchin, T. Takizuka, H. Shirai, T. Fujita, A. Isayama, Y. Koide and Y. Kamada, *Plasma Phys. Control. Fusion* **43**, 661 (2001).
- ³² G.L. Jackson, J. Winter, T.S. Taylor, *et al.*, *Phys. Rev. Lett.* **67**, 3098 (1991).
- ³³ C.M. Greenfield, B. Balet, K.H. Burrell, *et al.*, *Plasma Phys. Control. Fusion B* **35**, 263 (1993).

³⁴ M.V. Andrejko, L.G. Askinazi, V.E. Golant, *et al.*, Plasma Phys. Control. Fusion A **36**, 165 (1994).

³⁵ P.H. Diamond, V.B. Lebedev, D.E. Newman, and B.A. Carreras, Phys. Plasmas **2**, 3685 (1995).